ments should be found as clasts in meteorite regolith breccias. Angrite-like material has not been found in the howardites or mesosiderites, which are thought to be surficial breccias of the eucrite parent body. However, angrite-like fragments have been found in polymict ureilites. Polymict ureilites may form the regolith of the ureilite parent body (*25*), thought to be similar in composition to CV or CO carbonaceous chondrites (*26, 27*). If so, it is possible that some basalts on the ureilite parent body are angritic rather than eucritic.

These experimental results indicate that the partial melting of chondritic sources may produce both eucritic and angritic magmas. The differences in major-element compositions between angritic and eucritic magmas are comparable to those between terrestrial tholeiites and alkali basalts. Our experiments show that these differences can be produced without recourse to high-pressure fractionation or volatile fluxing. The production of eucrites by simple partial melting can still be disputed (*13*), but the origin of angritic magmas by a similar mechanism has been hitherto unsuspected.

REFERENCES AND NOTES

1. G. W. Lugmair, S. J. G. Galer, R. Loss, *Lunar Planet. Sci.* **XX**, 604 (1989).
2. L. Nyquist, H. Wiesmann, B. Bansal, C.-Y. Shih, *ibid.*, p. 798.
3. R. N. Clayton and T. K. Mayeda, *Lunar Planet. Inst. Tech. Rep. 90-01* (1990), p. 30.
4. M. B. Duke and L. T. Silver, *Geochim. Cosmochim. Acta* **31**, 401 (1967).
5. M. Prinz *et al.*, *Earth Planet. Sci. Lett.* **35**, 317 (1977).
6. G. A. McKay, D. J. Lindstrom, S.-R. Yang, J. Wagstaff, *Lunar Planet. Sci.* **XIX**, 762 (1988).
7. G. A. McKay, G. Crozaz, J. Wagstaff, S.-R. Yang, L. Lundberg, *ibid.* **XXI**, 771 (1990).
8. D. W. Mittlefehldt and M. M. Lindstrom, *Geochim. Cosmochim. Acta* **54**, 3209 (1990).
9. E. M. Stolper, *ibid.* **41**, 587 (1977).
10. R. Brett, J. S. Huebner, M. Sato, *Earth Planet. Sci. Lett.* **35**, 363 (1977).
11. G. A. McKay, L. Le, J. Wagstaff, *Lunar Planet. Sci.* **XX**, 675 (1989).
12. B. Mason, *Meteorites* (Wiley, New York, 1962).
13. R. H. Hewins and H. E. Newsom, in *Meteorites and the Early Solar System,* J. F. Kerridge and M. S. Matthews, Eds. (Univ. of Arizona Press, Tucson, 1989), pp. 73–101.
14. M. Prinz, M. K. Weisberg, C. E. Nehru, *Lunar Planet. Sci.* **XIX**, 949 (1988).
15. Allende sample 23A-S-1-H-4 was obtained from M. Zolensky, who in turn had received a larger sample from E. King. This sample is characterized in P. Johnson, thesis, University of Houston (1978).
16. G. A. McKay, D. J. Lindstrom, L. Le, S.-R. Yang, *Lunar Planet. Sci.* **XIX**, 760 (1988).
17. R. J. Williams and O. Mullins, Jr., *NASA TMX-58167* (Government Printing Office, Washington, DC, 1976), p. 34.
18. J. I. Goldstein *et al.*, *Practical Scanning Electron Microscopy* (Plenum, New York, 1977).
19. D. A. Kring and G. A. McKay, *Lunar Planet. Sci.* **XV**, 461 (1984).
20. A. J. G. Jurewicz and E. B. Watson, *Contrib. Mineral. Petrol.* **99**, 176 (1988).
21. B. O. Mysen and I. Kushiro, *Carnegie Inst. Washington Yearb.* **75**, 678 (1976).
22. B. M. French and H. P. Eugster, *J. Geophys. Res.* **70**, 1529 (1965).
23. J. H. Berkley and J. H. Jones, *ibid.* **87** (suppl.), A 353 (1982).
24. T. M. McCord, J. B. Adams, T. V. Johnson, *Science* **168**, 1445 (1970).
25. M. Prinz, M. K. Weisberg, C. E. Nehru, J. S. Delaney, *Lunar Planet. Sci.* **XVII**, 681 (1986).
26. J. T. Wasson, C.-L. Chow, R. W. Bild, P. A. Baedecker, *Geochim. Cosmochim. Acta* **40**, 1449 (1976).
27. H. Higuchi *et al.*, *ibid.*, p. 1563.
28. K. C. Cox, J. D. Bell, R. J. Pankhurst, *The Interpretation of Igneous Rocks* (Allen & Unwin, London, 1979).

6 November 1990; accepted 19 February 1991

Three-Dimensional Structure of Recombinant Human Interferon-γ

STEVEN E. EALICK,* WILLIAM J. COOK, SENADHI VIJAY-KUMAR, MIKE CARSON, TATTANAHALLI L. NAGABHUSHAN, PAUL P. TROTTA, CHARLES E. BUGG

The x-ray crystal structure of recombinant human interferon-γ has been determined with the use of multiple-isomorphous-replacement techniques. Interferon-γ, which is dimeric in solution, crystallizes with two dimers related by a noncrystallographic twofold axis in the asymmetric unit. The protein is primarily α helical, with six helices in each subunit that comprise ~62 percent of the structure; there is no β sheet. The dimeric structure of human interferon-γ is stabilized by the intertwining of helices across the subunit interface with multiple intersubunit interactions.

INTERFERON-γ (IFN-γ) IS A PRODUCT of activated T lymphocytes and natural killer (NK) cells that was originally described as an antiviral agent (*1*). IFN-γ exhibits pleiotropic biological activities (*2*) and specifically has been shown to regulate expression of class II major histocompatibility antigens (*3*) and Fc receptors (*4*), activate human monocyte cytotoxicity (*5*), enhance NK cell activity (*6*), and regulate immunoglobulin production and class switching (*7*). Expression of biological activity appears to be mediated through binding to specific cell-surface receptors (*8*), which have been cloned (*9*). The expression of human IFN-γ in *Escherichia coli* (*10, 11*) has resulted in the preparation of large quantities of highly purified recombinant human IFN-γ on which detailed studies of structure-function relations have been initiated (*12–16*).

We reported a preliminary crystallographic study of an *E. coli*–derived recombinant form of human IFN-γ, designated IFN-γ D′, in which the five COOH-terminal residues are deleted (*17, 18*). We report here the determination of the three-dimensional (3-D) structure of recombinant human IFN-γ D′ with the use of multiple isomorphous replacement (MIR) techniques (*19, 20*).

Screening for heavy-atom derivatives was done initially by film methods with synchrotron radiation and subsequently with a Nicolet X-100A area detector (*21*). Eight heavy-atom derivatives were identified, all of which contained multiple sites that made the difference Patterson maps difficult to interpret. Fortunately, one of the derivatives [1 mM $KAu(CN)_2$] contained one site of much higher relative occupancy that could be identified with certainty from the Patterson map. Phases were calculated based on the Au derivative, and the heavy-atom sites of the other derivatives were then located from cross-difference Fourier maps. Heavy-atom parameters were refined with the use of the centric data (Table 1) (*22*); none of the eight derivatives was of high quality. The overall figure-of-merit for data to 3.5 Å resolution for all eight derivatives was 0.74.

Prior to calculation of an electron density map, the phases were improved by solvent-flattening techniques with the ISIR/ISAS package of programs by Wang (*23*). The initial molecular envelope was determined by assuming a solvent fraction of 50%. After convergence, the overall figure-of-merit was 0.85, the average accumulated phase shift was 21°, the R factor between calculated structure factors (F_c) after map inversion and observed structure factors (F_o) was 0.282, and the correlation coefficient between F_o and F_c was 0.95. The electron density map calculated with these phases

S. E. Ealick, Department of Pharmacology, Center for Macromolecular Crystallography and Comprehensive Cancer Center, University of Alabama at Birmingham, Birmingham, AL 35294.
W. J. Cook, Department of Pathology, Center for Macromolecular Crystallography and Comprehensive Cancer Center, University of Alabama at Birmingham, Birmingham, AL 35294.
S. Vijay-Kumar and M. Carson, Center for Macromolecular Crystallography, University of Alabama at Birmingham, Birmingham, AL 35294.
T. L. Nagabhushan and P. P. Trotta, Schering-Plough Research, Bloomfield, NJ 07003.
C. E. Bugg, Department of Biochemistry, Center for Macromolecular Crystallography and Comprehensive Cancer Center, University of Alabama at Birmingham, Birmingham, AL 35294.

*To whom correspondence should be addressed.

was quite noisy, and the noncrystallographic symmetry was poor. Therefore, the noncrystallographic twofold axes were derived by averaging the positions of the heavy atoms in the various derivatives, and the electron density was then averaged based on the noncrystallographic symmetry.

This map clearly showed the protein-solvent boundary and two dimers that were related by a noncrystallographic twofold axis. All 12 α helices in the dimer could be seen in this map. Four loop regions linking five of the helices were also visible in the map. Two regions of the polypeptide chain, the long loop between helices A and B and the last 15 residues at the COOH-terminus, appear to be disordered or highly flexible because the electron density is weak.

Preliminary refinement of a starting model (*24*) with the method of simulated annealing with the program XPLOR (*25*) gave an *R* factor of 0.25 with 6.0 to 2.8 Å data (13,192 reflections > 2σ; 4,072 atoms). Portions of helices B, C, and D with the associated 3.5 Å MIR electron density that has been solvent flattened and symmetry averaged are shown in Fig. 1. The final model contains 123 residues and is complete except for the COOH-terminal residues 124 and 138; residues 122 to 138 probably extend away from the dimer. The root-mean-square differences between Cα carbons of individual subunits after refinement without the use of noncrystallographic symmetry restraints ranged from 0.8 to 1.2 Å. There were no significant differences between subunits in the same dimer compared to subunits in separate dimers.

Recombinant human IFN-γ D′ is a dimer with identical subunits that are related by a noncrystallographic twofold axis (Fig. 2). The dimer is globular with overall dimensions of approximately 60 Å by 40 Å by 30 Å. The asymmetric unit contains two dimers related by a noncrystallographic twofold axis. Thus, the overall noncrystallographic symmetry is described by the point group 222 (*26*).

Each subunit of IFN-γ contains six α helices that comprise ~62% of the structure (Fig. 3). The helices range in length from 9 to 21 residues. All 12 helices in the dimer are generally parallel to the dimer twofold axis. There are no clear antiparallel four-helix domains in the molecule. Within the dimer, both parallel and antiparallel interactions are observed between adjacent helices. In addition, extensive interhelical contacts occur between helices in different subunits. The first four helices from one subunit form a cleft that accommodates the COOH-terminal helix from the other subunit (Fig. 4A). The COOH-terminal helix shows a bend in the center at residue Glu^{112} with an

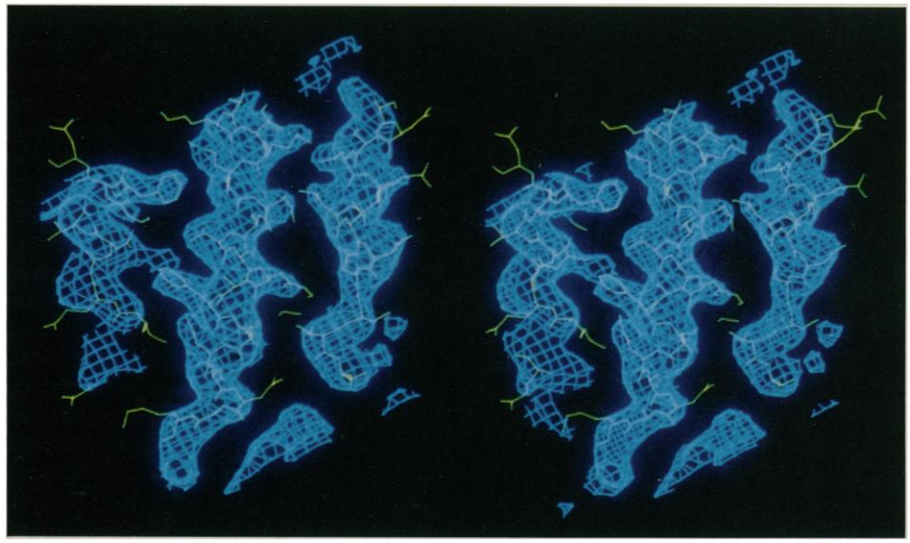

Fig. 1. Stereo view of a portion of the IFN-γ D′ dimer with the associated 3.5 Å MIR electron density modified by solvent flattening and symmetry averaging. From left to right, the figure includes residues 71 to 83 and 42 to 61 from one subunit and 89 to 101 from the other.

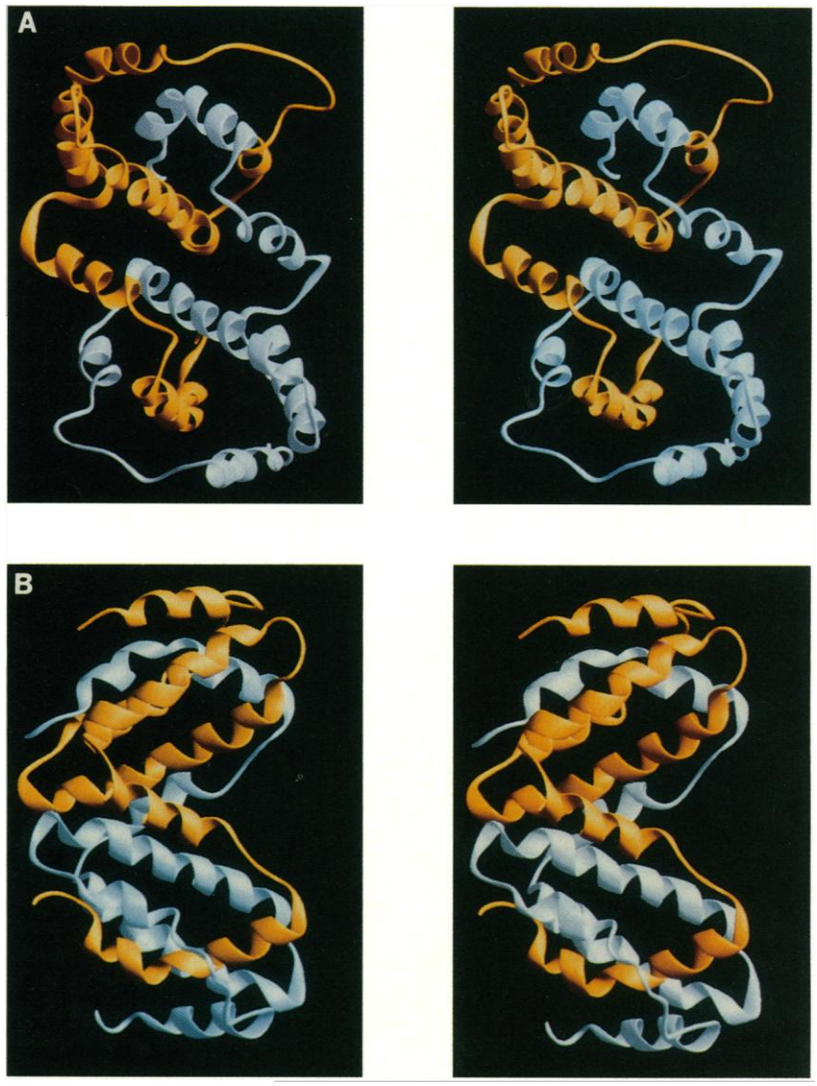

Fig. 2. Stereo views of the IFN-γ D′ dimer. The ribbon drawing is based on the Cα positions. (**A**) The view is approximately parallel to the dimer twofold axis. (**B**) The view is approximately perpendicular to the dimer twofold axis.

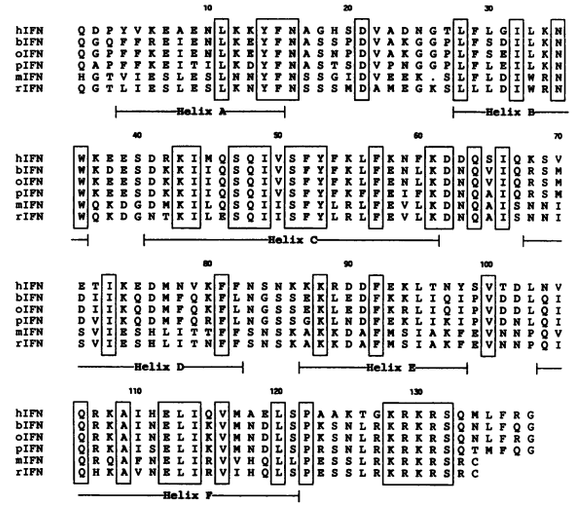

Fig. 3. Amino acid sequences of IFN-γ derived from the human (*11*), bovine (*39*), sheep (*40*), pig (*41*), mouse (*42*), and rat (*43*) cDNA sequences (*44*). The α-helical assignments based on the IFN-γ D′ structure are noted beneath the residues. The bovine, ovine, and porcine sequences have been truncated at the COOH-terminus to correspond to the recombinant human IFN-γ D′ sequence. There is a deletion in the mouse sequence corresponding to position 26 in the human sequence.

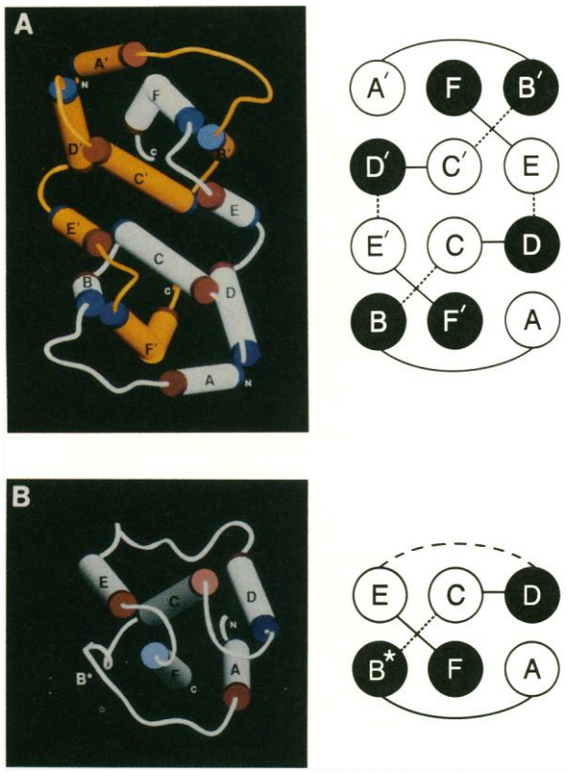

Fig. 4. Schematic drawings of (**A**) the recombinant human IFN-γ D′ dimer and (**B**) IFN-β. On the left-hand side, the α helices are represented as cylinders, and the nonhelical regions are shown as tubes. The NH_2- and COOH-terminal ends of the helices are colored blue and red, respectively. On the right-hand side, the α helices are represented as circles, and the nonhelical regions are shown as solid or dashed lines, depending on whether they are above or below the plane of the figure. The NH_2-terminal ends of the helices are darkened. The regions labeled B* represent a kinked region of IFN-β that is not helical but shows some helical features.

Table 1. Summary of data collection and analysis of heavy-atom derivatives in which 10 to 3.5 Å area-detector data were used. The number in parentheses after the number of unique reflections is the percent completeness of the data. R_{merge} is reported for intensities. R_F is the percentage change between native (F_1) and scaled derivative (F_2) data $[(\Sigma||F_1| - |F_2||)/\Sigma|F_1|]$. F_H/E is the average value of the heavy-atom contribution divided by lack-of-closure error. No Au position was identified in the combined Pt-Au heavy-atom soak.

Data	Reso-lution (Å)	Observations (no.)		R_{merge}	R_F	F_H/E
		Total	Unique			
Native (7)*	2.8	158,195	19,954(96)	11.3		
$KAu(CN)_2$, 1 mM (3)	3.1	42,557	13,189(86)	9.9	9.5	1.0
$KAu(CN)_2$, 5 mM (1)	3.1	56,296	14,379(99)	9.3	20.6	1.0
$K_2Pt(CN)_4$ (1)	3.0	61,888	15,513(96)	9.2	14.1	0.9
K_2HgI_4 (2)	3.4	17,051	9,929(85)	8.9	31.2	1.1
K_2PtCl_4 (1)	3.4	47,653	10,343(92)	9.9	20.6	1.0
$K_2Pt(NO_2)_4$ (7)	3.3	89,359	12,385(98)	9.5	21.1	1.0
$K_2Pt(NO_2)_4$ + $KAu(CN)_2$ (1)	3.35	47,679	11,008(95)	11.0	24.1	1.1
Na_2IrCl_6 (1)	3.6	21,571	6,551(70)	11.9	22.0	1.0

*Number of crystals.

angle between the two segments of ~125°. This pronounced bend may result from the large number of contacts between the helix and the cleft. There are hydrophobic contacts among all of the helices, but most are between the C and D helices. The C helix is the most hydrophobic helix in the subunit and is essentially buried in the core of the dimer.

The structure of the subunit is extended and has a flattened prolate elliptical shape. However, the two subunits are intimately related, and the overall structure is compact and globular. It is difficult to see how the dimer could be separated without significant disruptions in the tertiary structures of the individual subunits. The dimer interface is centered on helix C. The two symmetry-related C helices pack against each other with an angle of ~55°. Helices E and F from the other subunit flank either side of helix C. Intersubunit contacts also occur between the NH_2-terminal helix of one subunit and the COOH-terminal helix of the other. There is no β-sheet structure within the subunit or across the dimer interface.

Human IFN-γ contains two Asn-X-Ser/Thr glycosylation sites in the mature protein (*27*). One occurs at residues 25 to 27 at the end of the long flexible loop between helices A and B. The other occurs at residues 97 to 99 at the end of helix E. Both of these regions are on the surface of the molecule and are exposed to the solvent.

The dimeric structure of IFN-γ D′ is consistent with sedimentation equilibrium experiments which show that a similar form of human IFN-γ is dimeric in solution (*28, 29*), rather than trimeric or tetrameric (*30*). Unlike the *E. coli*–derived material described here, native human IFN-γ contains N-linked carbohydrate and is also heterogeneous at the COOH-terminus, exhibiting variable degrees of COOH-terminal processing (*27*). However, since the absence of carbohydrate does not significantly alter the conformation of human IFN-γ, and because the removal of up to 13 amino acid residues from the COOH-terminus does not affect either self-association or conformation (*14*), the dimeric structure and high α-helical content noted for recombinant human IFN-γ D′ are probably characteristic of native human IFN-γ. The dimeric structure of IFN-γ D′ is unusual among globular proteins in the way in which the subunits are so intimately linked. This type of intertwining between subunits has been reported for Trp repressor, which is also a dimer in which the subunits are primarily α helical (*31*).

Based on the current assignments of secondary structure, human IFN-γ D′ contains ~62% α helix and no β sheet. These data agree with analyses of far-ultraviolet circular

dichroic spectra that estimate an α-helix content of 40 to 66% and a low percentage of β sheet (*12, 29, 32*). However, IFN-γ D′ has no apparent homology with any previously reported α-helical proteins. On the basis of the location of the exon boundaries, loops are predicted to occur at or near residues 15, 38, and 99 (*33*), which agrees well with the observed secondary structure assignments (Fig. 3).

Residues at both the NH_2- and COOH-termini of human IFN-γ may be critical in the interaction with the receptor or triggering of biological response or both. For example, forms of recombinant human IFN-γ truncated at the COOH-terminus demonstrate substantially reduced antiviral activity (*13–16*), and antibodies directed to both the NH_2-terminus (*34, 35*) and COOH-terminus (*15, 35*) neutralize in vitro bioactivity. We conclude that the receptor-binding region requires an intact dimer and may include the COOH-terminus of one subunit and the NH_2-terminus of the other.

Truncation at the NH_2-terminus appears to result in a dramatic loss in secondary structure (*12*). The NH_2-terminus of one subunit has multiple contacts with helix D of the same subunit and helix F of the other subunit, and hence this region is necessary for maintenance of the overall structure. In addition, the NH_2-terminal helix of one subunit is required to maintain the cleft that accommodates the COOH-terminal helix of the other subunit.

Comparison of the amino acid sequences for IFN-γ from different mammalian species shows considerable homology (Fig. 3). Based on this homology, we expect that these IFN-γ's would have similar tertiary structures. Three of the most highly conserved regions in the sequences occur in helices C and F, which are the two most buried helices in the dimer, and a short basic stretch at the beginning of the COOH-terminal tail. Deletion mutants of human IFN-γ truncated at the COOH-terminus begin to show loss of activity when residues in this region are removed (*13–16*). One of the most variable regions is the loop between helices A and B. This loop may account for the high species specificity of IFN-γ; that is, IFN-γ from one species generally displays poor affinity for the receptor from another species.

To date, x-ray structures of three monomeric α-helical cytokines, growth hormone (*36*), interleukin-2 (*37*), and interferon-β (*38*), have been reported. As a dimeric cytokine IFN-γ represents a new structural class. Even so, comparison of the 3-D structures of IFN-γ and IFN-β reveals a striking similarity in folding topology (Fig. 4). Five of the 12 helices in the IFN-γ dimer (A, C, D, E′, and F′) form a structural domain that corresponds to the five helices of the IFN-β molecule. In addition, the short helix B of IFN-γ corresponds to a kinked region of IFN-β (B*) that displays some helical structure. Although the helices of IFN-β are somewhat more parallel to each other than are the helices of IFN-γ, the overall geometrical arrangement and connectivity are conserved. A long loop between helices D and E facilitates the monomeric structure of IFN-β, whereas in IFN-γ this loop is replaced by a tight turn that causes helices E and F to extend into the second subunit. This striking similarity in the 3-D structures of IFN-β and IFN-γ provides evidence for a common ancestral gene, even though no significant homology exists between their amino acid sequences and each molecule has a separate cellular receptor and biological function.

REFERENCES AND NOTES

1. E. F. Wheelock, *Science* **149**, 310 (1965).
2. R. Dijkmans and A. Billiau, *Curr. Opin. Immunol.* **1**, 269 (1988); H. W. Murray, *Ann. Intern. Med.* **108**, 595 (1988); G. Trinchieri and B. Perussia, *Immunol. Today* **6**, 131 (1985).
3. G. H. W. Wong, I. Clark-Lewis, J. L. McKimm-Breschkin, A. W. Harris, J. W. Schrader, *J. Immunol.* **131**, 788 (1983).
4. K. Itoh, M. Inoue, S. Kataoka, K. Kumagai, *ibid.* **124**, 2589 (1980).
5. C. F. Nathan, H. W. Murray, M.E. Wiebe, B. Y. Rubin, *J. Exp. Med.* **158**, 670 (1983).
6. C. D. Platsoucas, in *Natural Killer Activity and Its Regulation*, T. Hoshino, H. S. Koren, A. Uchida, Eds. (Excerpta Medica, Amsterdam, 1984), pp. 161–166.
7. F. D. Finkelman, I. M. Katona, T. R. Mosmann, R. L. Coffman, *J. Immunol.* **140**, 1022 (1988).
8. P. Anderson, Y. K. Yip, J. Vilcek, *J. Biol. Chem.* **257**, 11301 (1982).
9. M. Aguet, Z. Dembic, G. Merlin, *Cell* **55**, 273 (1988); V. Jung *et al.*, *ibid.* **265**, 1827 (1990).
10. P. W. Gray *et al.*, *Nature* **295**, 503 (1982).
11. S. Tanaka *et al.*, *Nucleic Acids Res.* **11**, 1707 (1983).
12. H. H. Hogrefe *et al.*, *J. Biol. Chem.* **264**, 12179 (1989).
13. P. O. Leinikki, J. Calderon, M. H. Luquette, R. D. Schreiber, *J. Immunol.* **139**, 3360 (1987).
14. T. Arakawa, Y.-R. Hsu, C. G. Parker, P.-H. Lai, *J. Biol. Chem.* **261**, 8534 (1986).
15. G. F. Seelig, J. Wijdenes, T. L. Nagabhushan, P. P. Trotta, *Biochemistry* **27**, 1981 (1988).
16. P. P. Trotta, G. F. Seelig, H. V. Le, T. L. Nagabhushan, *UCLA (Univ. Calif. Los Angel.) Symp. Mol. Cell. Biol. New Ser.* **50**, 497 (1986).
17. S. Vijay-Kumar *et al.*, *J. Biol. Chem.* **262**, 4804 (1987).
18. Recombinant IFN-γ D′ was expressed in *E. coli* by procedures similar to those previously described by Tanaka *et al.* (*11*). It was purified to constant-specific antiviral activity and apparent homogeneity with SDS–polyacrylamide gel electrophoresis by using standard chromatographic procedures. [H. V. Le, C. A. Mays, R. Syto, T. L. Nagabhushan, P. P. Trotta, in *The Biology of the Interferon System 1985*, W. E. Stewart II and H. Schellekens, Eds. (Elsevier, Amsterdam, 1985), pp. 73–80].
19. Crystals for x-ray diffraction studies were grown from 40% saturated ammonium sulfate solutions at pH 5.9 (*17*). The native data was obtained in part by using crystals grown under microgravity conditions on space shuttle mission STS-26 (*20*). The space group is *R*32 with hexagonal cell parameters $a = b = 114.0$ Å and $c = 315.0$ Å. The corresponding rhombohedral axes are $a = 123.9$ Å and $\alpha = 54.8°$. There are two dimers in the asymmetric unit, and the solvent volume fraction is ~60%.
20. L. J. DeLucas *et al.*, *Science* **246**, 651 (1989).
21. Potential heavy-atom derivatives were prepared by soaking crystals for 24 hours at 22°C in 65% ammonium sulfate solutions that contained 0.05 M MES, pH 5.9. Data for native crystals and the heavy-atom derivatives were collected by using CuKα radiation from a Rigaku RU-300 rotating anode x-ray source operating at 40 kV and 100 mA. Oscillation frames covered 0.25° and were measured for 5 min. In order to obtain complete data sets with multiple measurements of all reflections, multiple crystals were often used. Indexing and integration of intensity data were carried out with the XENGEN processing programs [A. J. Howard *et al.*, *J. Appl. Crystallogr.* **20**, 383 (1987)].
22. The derivatives are divided into two groups based on the sites of heavy-atom binding. The first group consists of $K_2Pt(NO_2)_4$, K_2PtCl_4, and Na_2IrCl_6. Each of these derivatives displays one binding site per subunit with the four binding sites related by 222 noncrystallographic symmetry. The heavy-atom sites for these derivatives are essentially the same. The derivatives show some variation in quality, with the $K_2Pt(NO_2)_4$ derivative being slightly better than any of the other three. The second group of heavy-atom derivatives consists of $KAu(CN)_2$, $K_2Pt(CN)_4$, and K_2HgI_4. As was the case for the first group of derivatives, each subunit contains one binding site, with the four resulting sites related by noncrystallographic symmetry. The 1 mM $KAu(CN)_2$ derivative has one site that appears to have much greater affinity than the other three sites within the crystallographic tetramer.
23. B. C. Wang, *Methods Enzymol.* **115**, 90 (1985).
24. One of the four polypeptide chains was traced from this map and then aligned with the amino acid sequence of the portions of the chain where the electron density was well defined. A starting model including all main-chain and side-chain atoms was built automatically from the initial Cα positions with a modified version of the fragment-fitting routines of T. A. Jones and S. Thirup [*EMBO J.* **5**, 819 (1986)]. The other three polypeptides were generated by using the noncrystallographic symmetry. Each residue was then fit to the unaveraged electron density with the aid of a local version of the graphics program TOM [C. Cambillau and E. Horjales, *J. Mol. Graphics* **5**, 174 (1987)], insuring that each side-chain and main-chain dihedral angle had a reasonable value.
25. A. T. Brünger, J. Kuriyan, M. Karplus, *Science* **235**, 458 (1987).
26. The crystal packing mimics the cubic space group *F*432 as a result of the arrangement of the noncrystallographic twofold axes. The coordinates of the atoms in the pseudocubic cell are related to those in the rhombohedral cell by the following transformation matrix:

$$\begin{vmatrix} a_c \\ b_c \\ c_c \end{vmatrix} = \begin{vmatrix} \frac{1}{2} & -\frac{1}{2} & 1 \\ 0 & \frac{1}{2} & 1 \\ -\frac{1}{2} & 0 & 1 \end{vmatrix} \begin{vmatrix} a_r \\ b_r \\ c_r \end{vmatrix} + \begin{vmatrix} \frac{1}{4} \\ \frac{1}{4} \\ \frac{1}{4} \end{vmatrix}$$

where the translation vector $(\frac{1}{4}, \frac{1}{4}, \frac{1}{4})$ reflects the difference in origin definition between *R*32 and *F*432. When this transformation matrix is applied to the center of the four subunits, one obtains approximately the 222 special position in the cubic space group. If the space group had been *F*432, there would have been one subunit per asymmetric unit.
27. E. Rinderknecht, B. H. O'Connor. H. Rodriguez, *J. Biol. Chem.* **259**, 6790 (1984).
28. D. A. Yphantis and T. Arakawa, *Biochemistry* **26**, 5422 (1987).
29. T. Arakawa, Y.-R. Hsu, D. A. Yphantis, *ibid.*, p. 5428.
30. S. Pestka *et al.*, *J. Biol. Chem.* **258**, 9706 (1983).
31. R. W. Schevitz, Z. Otwinowski, A. Joachimiak, C. L. Lawson, P. B. Sigler, *Nature* **317**, 782 (1985).
32. W. T. Windsor and P. P. Trotta, unpublished observations.
33. P. W. Gray and D. V. Goeddel, *Nature* **298**, 859 (1982).
34. H. I. Magazine *et al.*, *Proc. Natl. Acad. Sci. U.S.A.*

85, 1237 (1988); M. P. Langford *et al., Biochem. Biophys. Res. Commun.* **117**, 866 (1983); H. M. Johnson, M. P. Langford, B. Lakhchaura, T.-S. Chan, G. J. Stanton, *J. Immunol.* **129**, 2357 (1982).
35. G. F. Seelig *et al., J. Interferon Res.* **9** (suppl. 2), S184 (Abst. A4-20) (1989).
36. S. S. Abdel-Meguid *et al., Proc. Natl. Acad. Sci. U.S.A.* **84**, 6434 (1987).
37. B. J. Brandhuber, T. Boone, W. C. Kenney, D. B. McKay, *Science* **238**, 1707 (1987).
38. T. Senda *et al., Proc. Jpn. Acad. Ser. B Phys. Biol. Sci.* **66**, 77 (1990).
39. P. W. Gray and D. V. Goeddel, in *Molecular Cloning and Analysis of Lymphokines,* D. R. Webb and D. V. Goeddel, Eds. (Academic Press, New York, 1987), pp. 151–161.
40. C. J. McInnes, M. Logan, J. Redmond, G. Entrican, G. D. Baird, *Nucleic Acids Res.* **18**, 4012 (1990).
41. R. Dijkmans, K. Vandenbroeck, E. Beuken, A. Billiau, *ibid.*, p. 4259.
42. P. W. Gray and D. V. Goeddel, *Proc. Natl. Acad. Sci. U.S.A.* **80**, 5842 (1983).
43. R. Dijkema *et al., EMBO J.* **4**, 761 (1985).
44. Abbreviations for the amino acid residues are A, Ala; C, Cys; D, Asp; E, Glu; F, Phe; G, Gly; H, His; I, Ile; K, Lys; L, Leu; M, Met; N, Asn; P, Pro; Q, Gln; R, Arg; S, Ser; T, Thr; V, Val; W, Trp; and Y, Tyr.
45. The α-carbon coordinates for recombinant human IFN-γ D′ will be deposited with the Brookhaven Protein Data Bank. We thank S. K. Narula and staff for the expression of recombinant human IFN-γ D′ in *Escherichia coli,* G. F. Seelig and P. Reichert for preparation of purified protein, S. Senadhi for preparation of recombinant human IFN-γ D′ crystals, and C. Smith and B. Cole for assistance with data processing. Supported by NIH grant CA-13148 and NASA grant NAGW813.

19 October 1990; accepted 20 February 1991

Fatal Sibling Aggression, Precocial Development, and Androgens in Neonatal Spotted Hyenas

LAURENCE G. FRANK, STEPHEN E. GLICKMAN, PAUL LICHT

Fatal neonatal sibling aggression is common in predatory birds but has not been previously reported in wild mammals. Spotted hyena females are strongly masculinized, both anatomically and behaviorally, apparently by high levels of androgens during ontogeny. Neonates display elevated androgen levels, precocial motor development, and fully erupted front teeth. Litters are usually twins, and siblings fight violently at birth, apparently leading to the death of one sibling in same-sex litters, whereas in mixed-sex litters both siblings usually survive.

SPOTTED HYENAS (*CROCUTA CROCUTA*) are the most abundant large terrestrial predators in sub-Saharan Africa. Their highly successful adaptations as social hunters include the behavioral dominance of females over males (*1*). Besides being heavier and more aggressive than males, females also have highly masculinized genitalia (*2*): the clitoris is greatly hypertrophied (the size of the male penis) and fully erectile. The vaginal labia are fused to form a scrotum. The urogenital canal traverses the clitoris, through which the female mates and gives birth.

A number of investigators have suggested (*3–5*) that "masculinization" of the female genitalia originated as a by-product of selection for secretion of androgens by female hyenas, resulting in increased body size and aggressiveness. The latter changes would be expected to enhance females' access to food during highly competitive feeding and thereby improve survival of offspring (*4, 5*). Selection would also operate on the by-products of such androgenization (for example, masculinization of genital morphology). Ability to participate in "meeting ceremonies," in which social cohesion is facilitated by mutual inspection of the erect genitals, was suggested as one such selective agent (*3*).

We describe another phenomenon that may have originated as a by-product of selection for female androgenization: extreme neonatal aggression that may culminate in the death of one member of the set of twins that normally constitute a litter.

Spotted hyenas weigh between 1.0 and 1.65 kg at birth and, unlike other carnivores (*6*), have fully erupted incisors and canines (Fig. 1). Their eyes are open and they are capable of strong, coordinated and highly directed behavior at birth. The stereotypic bite-shake attack that constitutes elevated aggression in adults commences in the first hour after birth. The prolonged gestation period of spotted hyenas, about 110 days, is presumably related to precocity. By contrast, in the striped hyena (*Hyaena hyaena*), gestation lasts about 90 days, incisors and canines erupt at 21 and 33 days, respectively, and the first social interactions, which are playful, appear at 30 days of age (*7*); females of this species do not exhibit masculinized genitalia.

Fig. 1. Dentition of spotted hyena on day of birth. Canines are 6 to 7 mm long; incisors 2 to 4 mm long.

We present data on fighting in five litters born at the University of California, Berkeley. The litters were videotaped for 12 to 24 hours per day from birth through 4 weeks of age: 121 to 147 hours per litter were analyzed (*8*). Unlike in the natural denning situation, the mother was accessible to the neonates 24 hours a day in the laboratory. Blood samples were taken at intervals through the first month after birth and analyzed (*9*) for androgens (testosterone and androstenedione).

Infants were delivered about 1 hour apart. The first born usually attacked the second within minutes of birth; in one case, the third born was attacked while still fully enclosed in its amniotic membrane. Aggression was most intense on the day of birth, falling rapidly thereafter (Fig. 2). Initially, all aggression consisted of bite-shakes, directed primarily at the neck and anterior dorsum. Fighting was initiated by the first born but quickly became mutual. One sibling established dominance over the other in the first days and thereafter bite-shakes were largely replaced by brief bites and threats. Beginning shortly after birth, a characteristic pattern of wounds could be observed on the back of the subordinate infant, although, in captivity, these only required medical treatment among triplets.

Plasma androgens are markedly elevated at birth in spotted hyenas. Plasma androstenedione (A) is similarly elevated in both sexes at birth, but it remains elevated during the first month in females whereas it falls progressively in males during the same time span (Fig. 3). Androstenedione, primarily of ovarian origin, remains the primary circulating androgen in nonpregnant adult females (*10*). In contrast, testosterone (T) is typically higher in males than in females throughout the first month after birth (Fig. 3).

The elevated androgens at birth are likely an extension of high levels in the maternal and fetal circulation during much of gesta-

L. G. Frank and S. E. Glickman, Department of Psychology, University of California, Berkeley, CA 94720.
P. Licht, Department of Integrative Biology, University of California, Berkeley, CA 94720.